Published in final edited form as:
*Circ Cardiovasc Imaging*. 2010 May ; 3(3): 314–322. doi:10.1161/CIRCIMAGING.109.918482.

# Rapid Three-Dimensional Phenotyping of Cardiovascular Development in Mouse Embryos by Micro-CT with Iodine Staining

**Karl Degenhardt, MD, PhD**[1,3,4], **Alexander C. Wright, PhD**[2,4], **Debra Horng, BSc**[2], **Arun Padmanabhan, BA**[1], and **Jonathan A. Epstein, MD**[1]

[1] Department of Cell and Developmental Biology, Penn Cardiovascular Institute, and the Institute for Regenerative Medicine, University of Pennsylvania, Philadelphia, PA 19104, USA

[2] Laboratory for Structural NMR Imaging, Department of Radiology, University of Pennsylvania Medical Center, Philadelphia, PA 19104, USA

[3] Division of Cardiology, Department of Pediatrics, Children's Hospital of Philadelphia, Philadelphia, PA 19104, USA

## Abstract

**Background—**Micro-computed tomography (micro-CT) has been used extensively in research to generate high-resolution three-dimensional images of calcified tissues in small animals nondestructively. It has been especially useful for the characterization of skeletal mutations, but limited in its utility for the analysis of soft tissue such as the cardiovascular system. Visualization of the cardiovascular system has been largely restricted to structures that can be filled with radiopaque intravascular contrast agents in adult animals. Recent *ex vivo* studies using osmium tetroxide, iodinated contrast agents, inorganic iodine and phosphotungstic acid have demonstrated the ability to stain soft tissues differentially, allowing for high inter-tissue contrast in micro-CT images. Here, we demonstrate the application of this technology for visualization of cardiovascular structures in developing mouse embryos using Lugol's solution (aqueous potassium iodide plus iodine).

**Methods and Results—**We show the optimization of this method to obtain *ex vivo* micro-CT images of embryonic and neonatal mice with excellent soft-tissue contrast. We demonstrate the utility of this method to visualize key structures during cardiovascular development at various stages of embryogenesis. Our method benefits from the ease of sample preparation, low toxicity, and low cost. Furthermore, we show how multiple cardiac defects can be demonstrated by micro-CT in a single specimen with a known genetic lesion. Indeed, a previously undescribed cardiac venous abnormality is revealed in a *PlexinD1* mutant mouse.

**Conclusions—**Micro-CT of iodine stained tissue is a valuable technique for the characterization of cardiovascular development and defects in mouse models of congenital heart disease.

### Keywords

Micro-CT; iodine; mouse; development; PlexinD1; congenital heart disease

Karl Degenhardt, 1140 BRB II/III, 421 Curie Blvd, Philadelphia, PA 19104, degenhardt@email.chop.edu (215) 573-1220 (Phone) (215), 898-9871 (Fax). Alexander Wright, Radiology, 1 Silverstein, 3400 Spruce Street, Philadelphia, PA 19104, alexander.wright@uphs.upenn.edu, (215) 349-5295 (Phone), (215) 662-7263 (Fax).
[4]These authors contributed equally to this work

**Conflict of Interest Disclosures:** None.

The ability to genetically manipulate the mouse has resulted in a powerful model system for the investigation of many disease processes. In particular, genetic studies in the mouse have enhanced our understanding of embryonic development, and by extension, of congenital defects. In humans, cardiac defects are the most common serious anomalies among live births with an estimated frequency of 0.6% [1]. Numerous mouse models of congenital heart disease have been generated and characterized, adding greater insight into the molecular and cellular origins of these defects [2]. In addition, current research in the area of targeted gene deletions holds great promise to further elucidate mechanisms of cardiac development.

Although structurally similar to the human, the significantly reduced size of the murine cardiovascular system presents a number of technical challenges when attempting to stage anatomical features such as vascular structures. Identification and characterization of the phenotype of cardiovascular defects in mice traditionally has relied upon histological analysis of sectioned specimens. Histology, however, is limited to fixed two-dimensional views from which critical information may be lost, and it is prone to artifacts associated with sample fixation and preparation. These limitations make the visualization of features such as ventricular septal defects or subtle vascular abnormalities challenging. Three-dimensional (3D) reconstruction of photomicrographs is possible, but is highly labor intensive [3, 4] and prone to many of the same artifacts. Episcopic fluorescence image capture (EFIC), on the other hand, is a promising new histological technique that can generate a 3D data set from sectioned material [5, 6]. Nevertheless, non-destructive imaging modalities, such as high frequency ultrasound [7, 8], micro-MRI [9–11], and micro-CT [12, 13], are available for assessing cardiovascular structural abnormalities in mice.

Micro-computed tomography (micro-CT) has been used widely for morphological phenotyping of calcified tissues, primarily bone in small animals *ex vivo*, providing true 3D visualization of microstructure at isotropic resolutions as high as 5–10 μm [14–16]. The great advantages of micro-CT are the non-destructive nature of the imaging, as compared to histologic techniques, and the relative speed of data acquisition, as compared with micro-MRI techniques [17, 18]. However, micro-CT has been limited to the imaging of calcified or otherwise radiopaque tissues, as soft tissues provide little relative contrast in the images. Although it has been possible to visualize microvasculature with micro-CT by *post mortem* perfusion of a radiopaque fluid [19–21], contrast between different soft tissues is not generally available due to similarity of their X-ray attenuation. Recently, however, the possibility of obtaining high relative tissue contrast with micro-CT was demonstrated by first soaking the tissue in a solution containing an element of high atomic number, for example osmium in an aqueous solution of osmium tetroxide [12, 22–24]. In addition, commercially available iodine-based contrast agents used in clinical CT imaging have been shown to accomplish similar results [25], allowing for the quantification of tissue properties such as fixed charge density [26]. Furthermore, inorganic iodine and phosphotungstic acid recently have been shown to provide adequate staining for the visualization of the developing chick embryo by micro-CT [13].

We have independently developed a similar process for treating embryonic tissue samples prior to micro-CT scanning. We demonstrate here the ability to generate contrast for micro-CT imaging of soft tissues using a radiopaque contrast agent: aqueous potassium tri-iodide ($K^+ + I_3^-$), also known as Lugol's solution, and we show optimization of this technique for maximum resolution of soft tissues in embryonic and newborn mice with minimal artifact. We provide a detailed description of our protocol and an atlas of mouse development as visualized by micro-CT. Furthermore, we demonstrate that this technique is suitable for analysis of cardiovascular structures at various embryonic stages during mouse development. Finally, using *PlexinD1* mutant mice as an example, we show that multiple cardiovascular defects can be illustrated in a single specimen, including a previously

unappreciated phenotype. Such a capability will be of great utility for the nondestructive visualization and characterization of mouse mutants that serve as models of congenital heart disease.

## Methods

### Iodine Staining Protocols

Mouse embryos were fixed overnight in 4% paraformaldehyde in phosphate-buffered saline (PBS), after which they were treated with Lugol's solution as a micro-CT contrast agent. Samples were soaked in various preparations of Lugol's solution for 24 to 72 hours. Lugol's solution, or Lugol's iodine [27], was prepared from 10 g KI plus 5 g $I_2$ in 100 ml $H_2O$. The potassium iodide in water dissociates, and upon adding elemental iodine the formation of the tri-iodide ion is favorable, enhancing the aqueous solubility of iodine. The traditional (100%) Lugol's solution thus has an iodine concentration of 986 mM and has an osmolarity of 1204 mOsmoles per liter, including all ionic species. However, normal saline (0.9% NaCl), which is physiologically isotonic, has an osmolarity of 308 mOsmoles per liter. Thus, a 25% Lugol's solution, made by diluting 100% Lugol's with de-ionized $H_2O$, will be approximately isotonic to biological tissues. Since hypertonic solutions have the tendency to cause tissue shrinkage due to the extraction of water from the tissue, we tested different treatments of the specimens using various mixtures of Lugol's solution and different durations of exposure of the specimens. The different treatments were qualitatively and quantitatively evaluated for degree of tissue shrinkage, soft tissue image contrast and signal to noise ratio, and uniformity of iodine penetration.

In order to quantify the apparent concentration of iodine in the tissues of each embryo, we first performed micro-CT scans on a set of calibration phantoms consisting of plastic tubes each filled with a different serial dilution, made with de-ionized water, from the same preparation of 100% Lugol's solution. Each tube was embedded in paraffin wax in a manner identical to that used for preparing embryos for micro-CT scanning. The mean reconstructed image intensity in Hounsfield units (HU) within a region of interest (ROI) drawn on each image was plotted versus its corresponding iodine concentration. A linear fit to the data points yielded the so-called "K factor" as the slope of the fitted line [28]. The equation of the fitted line thus provides a means to transform image intensity (HU) into apparent iodine concentration (mM) (Supplemental Figure 1). This provides only the apparent iodine concentration because no correction was made for the spectral filtering of the X-ray beam, i.e., beam hardening, caused by the sample [29].

Another means to evaluate the contrast agent is by measuring its effective diffusion coefficient $D$. To do this, a one-dimensional diffusion equation [30] can be applied approximately to the sample preparation technique, where contrast agent concentration at position $x$ in the tissue and at time $t$ is given by

$$C(x,t)=C_0 erfc(x/\sqrt{4Dt}) \qquad \text{Equation 1}$$

where *erfc* is the complementary error function. Here, the assumption is made that a semi-infinite half-space of contrast agent solution at concentration $C_0$ is adjacent to a homogeneous semi-infinite half-space of tissue, in which case only diffusion occurring along the $x$-axis, which is orthogonal to the interface, is relevant. By measuring the concentration of stain at a point $x$ in the tissue at various times $t$, we can fit this equation to the data points to obtain an estimate of the effective diffusion coefficient $D$. Equation 1 was fitted to data points obtained from each mouse neonate soaked in a different preparation of

Lugol's solution: isotonic 25% and 12.5% solutions, and a saturated 25% solution. 100% Lugol's solution was diluted 1:4 in de-ionized water giving it a calculated osmolarity of 308 mOsmoles per liter (isotonic 25%). This solution was, in turn, diluted 1:1 in isotonic PBS (isotonic 12.5%). Since elemental iodine ($I_2$) is relatively insoluble in water unless complexed with Ĩ, addition of $I_2$ crystals theoretically should not alter the osmolarity. We therefore also tested 25% Lugol's solution saturated with $I_2$ (saturated 25%). Specimens stained with each of these three solutions were imaged on three consecutive days after 24, 48 and 72 hours of treatment. A small circular ROI was drawn in the brain stem on a central sagittal slice of the micro-CT data acquired from each mouse at each time point to insure a repeatable location in the brain stem. The ROI had a diameter of 150 μm and its center (*x* position) and was about 600 μm from the skin surface. The brain stem was chosen for its uniform intensity and relatively superficial location in order to approximate the assumptions behind Equation 1.

### Micro-CT Scanning

The micro-CT scanner used in this study is an eXplore Locus SP specimen scanner (GE Healthcare), and has been described previously [31]. Resolution as high as 8x8x8 $\mu m^3$ can be achieved in reconstructed images of objects approximately 1 cm in diameter or less, while objects up to 3 cm in diameter can be accommodated with some loss of resolution. Raw projection data were acquired using the following parameters: 80 kVp, 80 μA, 400 views, 0.5° increment, short scan (Parker) method, 1.7 s exposure time, 2x2 pixel binning, 16 μm isotropic resolution, 8 frame averages, and 2 hr scan time. Since signal to noise ratio and achievable resolution are inversely related [31], the signal to noise ratio was increased by averaging together eight data acquisitions. The projection data were corrected for distortion and detector anomalies and then reconstructed by Feldkamp cone-beam filtered back-projection, resulting in a 3D image volume having isotropic resolution. Typical reconstructed voxel size was 16×16×16 $\mu m^3$, although some images were reconstructed at 32×32×32 $\mu m^3$. Intensity values in the reconstructed images conformed to the Hounsfield scale, with air set to −1000 HU and water set to 0 HU.

We embedded each embryo in paraffin wax in a small plastic test tube (inner/outer diameter = 10/12 mm) that fitted securely within the acrylic plastic sample tube supplied by the micro-CT scanner's manufacturer. Initial scanning experiments were performed without wax by wrapping the iodine-stained specimen in thin plastic wrap prior to inserting it into the acrylic sample tube. The plastic wrap prevented iodine from contaminating the walls of the plastic sample tube, however with this configuration there was the possibility of slight sample movement during the two-hour scan, leading to image blurring. Therefore instead of plastic wrap we used paraffin embedding of the sample in a smaller diameter tube that could be removed from the scanner's sample tube. The latter method worked better as it effectively immobilized the sample during the scan and avoided iodine contamination of the scanner's sample tube.

## Results

### Iodine Staining of Soft Tissues Produces Differential X-ray Attenuation on Micro-CT

In order to assess the ability of iodine to stain and penetrate tissue, fixed neonatal mice first were skinned and placed in mixtures of PBS and 100% Lugol's solution at various ratios for approximately 72 hours prior to imaging by micro-CT. Using pure PBS, only bony structures were clearly visualized (Figure 1A). However, with addition of a relatively small amount of Lugol's solution, differential staining of soft tissues occurred as evidenced by variable attenuation (Figure 1B). Increased proportions of Lugol's solution showed better differential staining, with liver and brown fat staining more intensely (Figure 1C and 1D).

Higher ratios of Lugol's also resulted in more uniform penetration, however a greater degree of tissue shrinkage was noted (compare Figure 1B and 1C). These solutions contained PBS, which is isotonic, plus Lugol's solution, which is hypertonic. The mixtures were therefore hypertonic, which we postulate may have contributed to tissue shrinkage and distortion.

In an effort to optimize the contrast observed by micro-CT, we next stained fixed neonatal mice in solutions that were physiologically isotonic, but of different iodine concentrations, for various periods of time (24, 48 and 72 hrs) prior to micro-CT imaging. With 12.5% Lugol's, uniform penetration of the specimen was not achieved, even after 72 hours of staining (Figure 2G-I). In contrast, saturated 25% Lugol's showed uniform penetration by 48 hours, but also began to show tissue distortion (shrinkage) by that time (Figure 2A-C). Staining with 25% Lugol's for 48 hours resulted in complete and uniform tissue penetration with minimal shrinkage (Figure 2E). Thus, for subsequent experiments we stained with 25% Lugol's solution for 48 hours prior to scanning. It should be noted that despite the use of isotonic solutions, some degree of tissue distortion always occurred under conditions that gave adequate differential staining.

All three isotonic solutions showed evidence of progressive diffusion as staining of the central portion of the specimen increased over time, with the time course varying by concentration (Figure 2). When the apparent iodine concentration in tissue (see Supplemental Figure 1) was plotted versus time, the one-dimensional diffusion equation (Equation 1) could provide a reasonably good approximation of the data (Figure 2J). The best fit of this equation gave an effective diffusion coefficient $D$ for each curve (Supplemental Table 1). The value of $D$ ranged from $3.95 \times 10^{-6}$ $mm^2/s$ to $5.99 \times 10^{-6}$ $mm^2/s$, approximately 250 times smaller than that for pure water. This is consistent with the observed delay in staining of the central portion of the embryo (Figure 2). The process of contrast optimization thus utilized both qualitative and quantitative analyses of the various staining protocols tested here.

### Iodine Staining Enables Visualization of Embryonic Mouse Development by Micro-CT

Micro-CT of iodine-stained mouse embryos at multiple developmental time points was performed using the staining protocol as optimized. Representative VR, MIP, and MPR sagittal views are shown (Figure 3 and Supplemental Figure 2). Differential staining of embryonic tissues was seen in specimens as young as embryonic day 11.5 post conception (E11.5). Embryos at E10.5 stained relatively weakly and displayed mostly uniform image intensity. Interestingly, blood stained most intensely at E11.5 (see Figure 3G-L, MIP images) and throughout development. Less intensely staining structures, such as somites, also could be distinguished easily from surrounding tissue (Figure 3N). In most specimens analyzed, the cardiac ventricles were partially or completely emptied of blood, leaving the chambers dark. Thus, trabeculation could be appreciated in many images. Due to space constraints, only a selection of sagittal views is shown. Complete images stacks can be viewed in Supplemental Movies 1–6.

Developing cardiovascular structures could be clearly appreciated by micro-CT. For example, at E11.5, both the truncus arteriosus and the ventricles are undergoing septation. The conotruncal region can be appreciated at early stages of septation (Figure 4A); the presumptive right and left ventricles have a partially formed septum, however the bulboventricular foramen remains (Figure 4A). By E13.5, the aorta and pulmonary artery are divided, while the ventricular septum is not yet complete (Figure 4B and 4C). Quantitative analysis of aortic vessel diameters measured from either histological cross-sections or micro-CT datasets of E17.5 embryos yielded comparable results (Supplemental Figure 3).

### Micro-CT of Iodine-Stained Blood Allows Three-Dimensional Angiography

As iodine stains blood intensely, micro-CT angiograms often could be generated without the need of injected contrast agents. Micro-CT data from a postnatal day 0 (P0) pup were used to generate a VR image of vascular structures that illustrates the similarities between human and mouse arterial structures and differences in venous structures (Figure 5). Mice have a left-sided aortic arch, with the same branching pattern as that seen in humans. Unlike humans, mice have bilateral superior vena cavae and a left-sided azygos vein. In addition, mice have a single pulmonary vein, rather than four separate veins entering the left atrium.

### Multiple Cardiac Defects Can Be Viewed by Micro-CT

Mice that are mutant for *PlexinD1* have been shown to have multiple cardiovascular defects, including truncus arteriosus, aberrant origins of the coronary arteries, and abnormal branching of the arch arteries [32]. We stained and imaged a *PlexinD1* null mutant embryo at E17.5 and compared it to a wild type embryo to see how each of these defects could be visualized. MPR was used to generate images at planes that best illustrate each of the defects. Corresponding views were made of the wild type control (Figure 6A-E). Truncus arteriosus was demonstrable along with a ventricular septal defect in an off-axis sagittal view (Figure 6F). A left arch with a retroesophageal right subclavian is best visualized in a cross-sectional view (Figure 6G). In other views, a coronary artery was shown with its origin at the sino-tubular junction, rather than in the sinus of Valsalva (Figure 6H). VR images were used to show the truncus arteriosus and arch branching (Figure 6I and 6J, and Supplemental Movies 7–8). Hence, both intracardiac and extracardiac defects can be effectively demonstrated by micro-CT.

In addition to visualizing previously reported cardiovascular defects, we were able to identify a novel abnormal cardiac venous connection in a *PlexinD1* mutant. Using multi-planar reformatting, an aberrant structure that appeared along the surface of the right ventricular outflow tract could be traced to the left superior vena cava (Figure 7A and Supplemental Movie 9). The structure ran along the left side of the truncus arteriosus. A similar cross-sectional view in the wild type control revealed no such structure (Figure 7B). This result suggests that *PlexinD1* is necessary not only for arterial patterning, but for venous patterning as well.

## Discussion

We have described here the ability to image soft tissues by micro-CT using aqueous potassium tri-iodide ($K^+ + I_3^-$), also known as Lugol's solution. Through the use of this stain, we have obtained excellent image contrast with micro-CT, allowing clear visualization of the heart and major vascular structures of neonatal and embryonic mice. Without iodine staining, the soft tissues of the mouse are iso-intense by micro-CT, however, many structures are dramatically revealed after treatment with Lugol's solution. Our initial experiments showed that differential staining of soft tissues was greater at higher iodine concentrations. However, these conditions also led to greater tissue distortion, evident by the increased spaces in the thoracic and abdominal cavities. This effect was reduced with the use of isotonic solutions and by limiting staining to 48 hours, although it appears that some degree of shrinkage was unavoidable under conditions that maximized differential staining. Nevertheless, the tissue distortion did not significantly interfere with qualitative analysis of cardiovascular structures. We note that Metscher evaluated the use of 10% Lugol's solution for micro-CT imaging of chick embryos [13], while we have arrived independently at a similar stain recipe (25% Lugol's solution) and optimized this protocol for mice. The structural similarity between the murine and human heart, in combination with the ability to manipulate the mouse genome, has made the mouse a widely used tool in cardiovascular

research. We conducted the present study with this in mind. The optimized micro-CT imaging protocol used here thus offers a fast, simple, and inexpensive method to characterize phenotypes in mouse models of cardiovascular development.

Shortening of the time needed for staining is limited by the diffusion properties of iodine. We were able to estimate the effective diffusion coefficient *D* by fitting a one-dimensional diffusion model to data points obtained from image intensities in the brain stems of mouse embryos subjected to different concentrations of iodine solution for different durations. The results indicated a relatively slow diffusion process, probably due to the existence of numerous barriers to iodine diffusion such as cell membranes and internal organ interfaces. The effective diffusion coefficients we estimated were consistent with the observed delay of staining in central portions of the specimens. The one-dimensional model used here (Equation 1) potentially could be improved by using a three-dimensional model having cylindrical geometry [30] or with additional dedicated experiments [33] beyond the scope of the present study.

The strength of any contrast agent lies in its ability to impart differential strength of signal. The images obtained here show that liver and brown fat stain strongly, but blood stains the most intensely. There are many gradations of lighter staining tissues as well. The brain and spinal cord stain moderately, with some distinction also evident between gray and white matter. Some muscles stain strongly, including the tongue and the myocardium. The inner walls of blood vessels are clearly visible when the lumen is not filled with blood and tracing the pattern of vessel branching can be easily accomplished. Likewise, when lumens are filled with blood, angiographic images can be generated. Depending on the desired anatomical image, specimen preparation may be modified to either allow blood to drain or not. For analysis of vascular anatomy, contrast also can be generated by *post mortem* perfusion of a radiopaque liquid (e.g., Microfil) consisting of a suspension of an element of high atomic number such as lead, bismuth or barium that solidifies prior to scanning. This has enabled micro-CT to become an excellent imaging tool for the characterization of, e.g., vascular patterning defects in a mouse model of human Notch signaling deficit [20]. However, such studies are limited to adult animals, as the immature vasculature of young animals does not tolerate the intravascular pressure needed to inject contrast. This is a particular problem in the study of cardiac development, since many cardiac defects result in embryonic or perinatal death, hence the strength of the micro-CT imaging protocol described here for imaging neonatal and embryonic mice.

*PlexinD1* mutant mice represent an example of a well-characterized genetic model of congenital heart disease that exhibits perinatal lethality (25). Plexins are cell surface receptors for semaphorin ligands that mediate guidance cues. The expression of *PlexinD1* on endothelial cells has been shown to be critical for normal cardiovascular development [32, 34]. Cardiovascular defects, including persistent truncus arteriosus, arch artery patterning defects, and aberrant coronary arteries, have been described previously (25). We have shown here the ability to thoroughly evaluate these cardiovascular defects, taking advantage of the ability to visualize the 3D data set from a single specimen from multiple angles. This approach is relatively simple and rapid, and proved sensitive enough to reveal a previously unappreciated abnormality of venous drainage in *PlexinD1* null mice. The association of coronary artery abnormalities with persistent truncus in patients has been long appreciated [35]. However, venous abnormalities in these same patients are less well described, and may deserve further investigation.

We were able to generate images of embryonic murine cardiovascular tissues with high inter-tissue contrast, similar to that of MRI yet in a fraction of the time. The primary advantages of micro-CT over MRI and other modalities are that micro-CT can generate

images at extremely high resolution (≤16 μm isotropic) of optically opaque samples in relatively short scan times (~ 2 hrs). The results presented here demonstrate the strength of micro-CT for visualizing soft tissues of the mouse at different embryonic stages. We have shown how micro-CT can be particularly applicable to the investigation of cardiac development and the analysis of mouse models of congenital heart disease. The technique is simple, fast, widely available and relatively inexpensive.

## Supplementary Material

Refer to Web version on PubMed Central for supplementary material.

## Acknowledgments

We thank Nicole Antonucci for assistance with animal care and husbandry.

**Funding Sources:** This work was supported by the National Institutes of Health (EB01427, P01HL075215, and T32HL007915), the American Heart Association (0440049N), and the Sarnoff Cardiovascular Research Foundation.

## References

1. Hoffman JI, Kaplan S. The incidence of congenital heart disease. J Am Coll Cardiol. 2002; 39:1890–1900. [PubMed: 12084585]
2. Horsthuis T, Christoffels VM, Anderson RH, Moorman AF. Can recent insights into cardiac development improve our understanding of congenitally malformed hearts? Clin Anat. 2009; 22:4–20. [PubMed: 19031393]
3. Kaufman MH, Brune RM, Davidson DR, Baldock RA. Computer-generated three-dimensional reconstructions of serially sectioned mouse embryos. J Anat. 1998; 193:323–336. [PubMed: 9877288]
4. Soufan AT, van den Berg G, Moerland PD, Massink MM, van den Hoff MJ, Moorman AF, Ruijter JM. Three-dimensional measurement and visualization of morphogenesis applied to cardiac embryology. J Microsc. 2007; 225:269–274. [PubMed: 17371450]
5. Dhanantwari P, Lee E, Krishnan A, Samtani R, Yamada S, Anderson S, Lockett E, Dono-frio M, Shiota K, Leatherbury L, Lo CW. Human cardiac development in the first trimester: a high-resolution magnetic resonance imaging and episcopic fluorescence image capture atlas. Circulation. 2009; 120:343–351. [PubMed: 19635979]
6. Rosenthal J, Mangal V, Walker D, Bennett M, Mohun TJ, Lo CW. Rapid high resolution three dimensional reconstruction of embryos with episcopic fluorescence image capture. Birth Defects Res C Embryo Today. 2004; 72:213–223. [PubMed: 15495188]
7. Manning WJ, Wei JY, Katz SE, Douglas PS, Gwathmey JK. Echocardiographically detected myocardial infarction in the mouse. Lab Anim Sci. 1993; 43:583–585. [PubMed: 8158984]
8. Gardin JM, Siri FM, Kitsis RN, Edwards JG, Leinwand LA. Echocardiographic assessment of left ventricular mass and systolic function in mice. Circ Res. 1995; 76:907–914. [PubMed: 7729009]
9. Smith BR. Magnetic resonance microscopy in cardiac development. Microsc Res Tech. 2001; 52:323–330. [PubMed: 11180623]
10. Schneider JE, Bamforth SD, Farthing CR, Clarke K, Neubauer S, Bhattacharya S. Rapid identification and 3D reconstruction of complex cardiac malformations in transgenic mouse embryos using fast gradient echo sequence magnetic resonance imaging. J Mol Cell Cardiol. 2003; 35:217–222. [PubMed: 12606262]
11. Petiet AE, Kaufman MH, Goddeeris MM, Brandenburg J, Elmore SA, Johnson GA. High-resolution magnetic resonance histology of the embryonic and neonatal mouse: a 4D atlas and morphologic database. Proc Natl Acad Sci U S A. 2008; 105:12331–12336. [PubMed: 18713865]
12. Johnson JT, Hansen MS, Wu I, Healy LJ, Johnson CR, Jones GM, Capecchi MR, Keller C. Virtual Histology of Transgenic Mouse Embryos for High-Throughput Phenotyping. PLoS Genetics. 2006; 2:e61. [PubMed: 16683035]

13. Metscher BD. MicroCT for developmental biology: a versatile tool for high-contrast 3D imaging at histological resolutions. Dev Dyn. 2009; 238:632–640. [PubMed: 19235724]
14. Engelke K, Graeff W, Meiss L, Hahn M, Delling G. High spatial resolution imaging of bone mineral using computed microtomography. Comparison with microradiography and undecalcified histologic sections. Invest Radiol. 1993; 28:341–349. [PubMed: 7683009]
15. Ritman EL. Molecular imaging in small animals--roles for micro-CT. J Cell Biochem Suppl. 2002; 39:116–124. [PubMed: 12552611]
16. Ford NL, Thornton MM, Holdsworth DW. Fundamental image quality limits for micro-computed tomography in small animals. Med Phys. 2003; 30:2869–2877. [PubMed: 14655933]
17. Johnson GA, Cofer GP, Gewalt SL, Hedlund LW. Morphologic phenotyping with MR microscopy: the visible mouse. Radiology. 2002; 222:789–793. [PubMed: 11867802]
18. Pieles G, Geyer SH, Szumska D, Schneider J, Neubauer S, Clarke K, Dorfmeister K, Franklyn A, Brown SD, Bhattacharya S, Weninger WJ. microMRI-HREM pipeline for high-throughput, high-resolution phenotyping of murine embryos. J Anat. 2007; 211:132–137. [PubMed: 17532797]
19. Jorgensen SM, Demirkaya O, Ritman EL. Three-dimensional imaging of vasculature and parenchyma in intact rodent organs with X-ray micro-CT. Am J Physiol. 1998; 275:H1103–1114. [PubMed: 9724319]
20. Proweller A, Wright AC, Horng D, Cheng L, Lu MM, Lepore JJ, Pear WS, Parmacek MS. Notch signaling in vascular smooth muscle cells is required to pattern the cerebral vasculature. Proc Natl Acad Sci U S A. 2007; 104:16275–16280. [PubMed: 17909179]
21. Gossl M, Rosol M, Malyar NM, Fitzpatrick LA, Beighley PE, Zamir M, Ritman EL. Functional anatomy and hemodynamic characteristics of vasa vasorum in the walls of porcine coronary arteries. Anat Rec A Discov Mol Cell Evol Biol. 2003; 272:526–537. [PubMed: 12740947]
22. Litzlbauer HD, Neuhaeuser C, Moell A, Greschus S, Breithecker A, Franke FE, Kummer W, Rau WS. Three-dimensional imaging and morphometric analysis of alveolar tissue from microfocal X-ray-computed tomography. Am J Physiol Lung Cell Mol Physiol. 2006; 291:L535–545. [PubMed: 16679382]
23. Faraj KA, Cuijpers VM, Wismans RG, Walboomers XF, Jansen JA, van Kuppevelt TH, Daamen WF. Micro-Computed Tomographical Imaging of Soft Biological Materials Using Contrast Techniques. Tissue Eng Part C Methods. 2009
24. Zhu XY, Bentley MD, Chade AR, Ritman EL, Lerman A, Lerman LO. Early changes in coronary artery wall structure detected by microcomputed tomography in experimental hypercholesterolemia. Am J Physiol Heart Circ Physiol. 2007; 293:H1997–2003. [PubMed: 17573460]
25. de Crespigny A, Bou-Reslan H, Nishimura MC, Phillips H, Carano RA, D'Arceuil HE. 3D micro-CT imaging of the postmortem brain. J Neurosci Methods. 2008; 171:207–213. [PubMed: 18462802]
26. Palmer AW, Guldberg RE, Levenston ME. Analysis of cartilage matrix fixed charge density and three-dimensional morphology via contrast-enhanced microcomputed tomography. Proc Natl Acad Sci U S A. 2006; 103:19255–19260. [PubMed: 17158799]
27. Kelly FC. Iodine in medicine and pharmacy since its discovery -- 1811-1961. Proc R Soc Med. 1961; 54:831–836. [PubMed: 19994130]
28. Takanami K, Higano S, Takase K, Kaneta T, Yamada T, Ishiya H, Mori I, Takahashi S. Validation of the use of calibration factors between the iodine concentration and the computed tomography number measured outside the objects for estimation of iodine concentration inside the objects: phantom experiment. Radiat Med. 2008; 26:237–243. [PubMed: 18509724]
29. Gillam JE, Kitcher D, Beveridge TE, Midgley S, Hall C, Lewis RA. K-edge subtraction using an energy-resolving position-sensitive detector. 2009
30. Crank, J. The Mathematics of Diffusion. 2. Oxford: Oxford University Press; 1979.
31. Marxen M, Thornton MM, Chiarot CB, Klement G, Koprivnikar J, Sled JG, Henkelman RM. MicroCT scanner performance and considerations for vascular specimen imaging. Med Phys. 2004; 31:305–313. [PubMed: 15000616]
32. Gitler AD, Lu MM, Epstein JA. PlexinD1 and semaphorin signaling are required in endothelial cells for cardiovascular development. Dev Cell. 2004; 7:107–116. [PubMed: 15239958]

33. Chowdhury MA, Hill DJ, Whittaker AK. NMR imaging of the diffusion of water at 37 degrees C into Poly(2-hydroxyethyl methacrylate) containing aspirin or vitamin B(12). Biomacromolecules. 2004; 5:971–976. [PubMed: 15132689]

34. Zhang Y, Singh MK, Degenhardt KR, Lu MM, Bennett J, Yoshida Y, Epstein JA. Tie2Cre-mediated inactivation of plexinD1 results in congenital heart, vascular and ske- letal defects. Dev Biol. 2009; 325:82–93. [PubMed: 18992737]

35. Shrivastava S, Edwards JE. Coronary arterial origin in persistent truncus arteriosus. Circulation. 1977; 55:551–554. [PubMed: 837493]

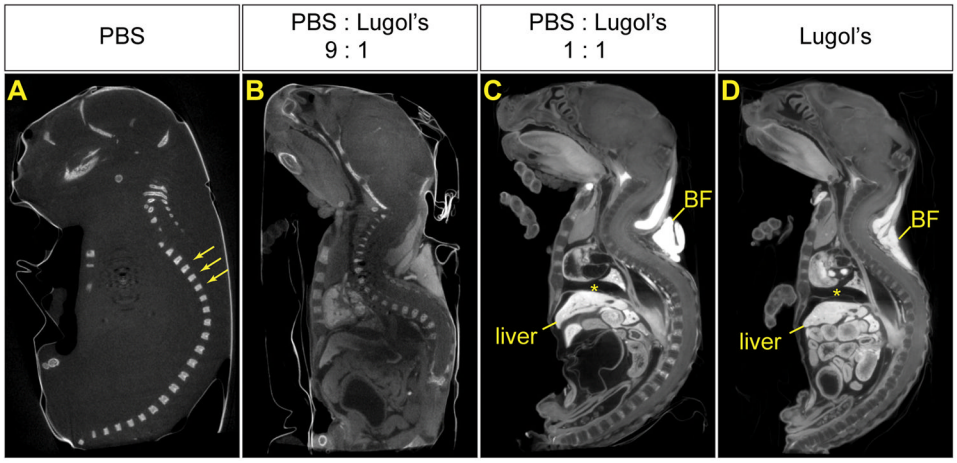


**Figure 1.**

Aqueous iodine stains soft tissue differentially in a concentration dependent manner. Four neonatal mice were treated with a mixture of PBS and 100% Lugol's solution in different ratios, prior to scanning by micro-CT. Representative sagittal MPR images are shown. Windowing for each image was separately optimized to maximize anatomic visibility. (**A**) Only calcified bony structures, such as vertebrae (arrows) are visible in a specimen treated in PBS alone. (**B**) The 9:1 mixture of PBS and Lugol's solution brings out many soft tissue structures, however, most tissues stain similarly and overall signal to noise ratio is poor. Moreover, the central part of the specimen remains unstained. (**C, D**) The 1:1 mixture of PBS and Lugol's solution (**C**) and 100% Lugol's solution (**D**) both impart differential attenuation to soft tissues, with brown fat (BF), liver and blood staining most intensely. However, there is some tissue distortion. Note the space between the diaphragm and heart (*).

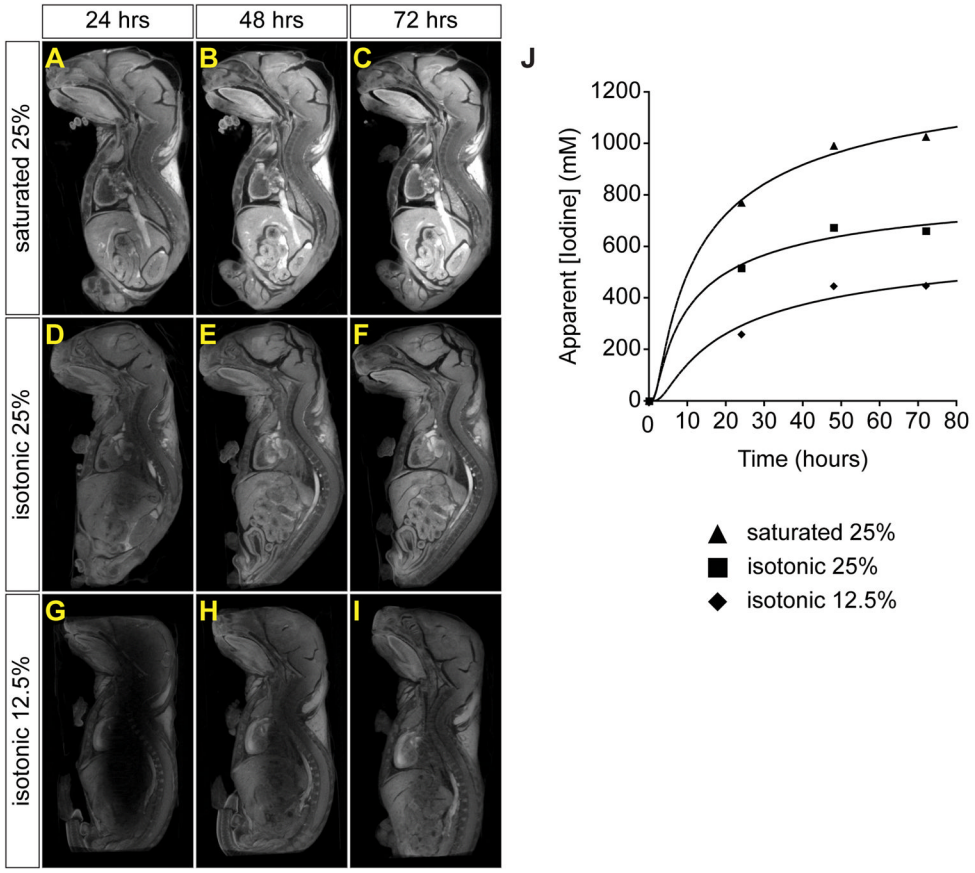


**Figure 2.**

The time course of progressive iodine diffusion and staining intensity varies with concentration of iodine in the stain solution. Three neonatal mice were stained with isotonic solutions of varying iodine concentrations and scanned by micro-CT serially over one (**A**, **D**, **G**), two (**B**, **E**, **H**) or three (**C**, **F**, **I**) days. Representative sagittal MPR images from three mouse neonates are shown. Windowing for all images is the same to allow comparison of staining intensity between panels. (**A-C**) Saturated 25% Lugol's gives rapid penetration and intense staining, however, significant shrinkage is seen. (**D-F**) Lugol's solution diluted to 25% in water shows good penetration by 48 hours with minimal tissue distortion. (**G-I**) 12.5% Lugol's solution fails to penetrate uniformly by 72 hours, but does show progressive diffusion of iodine into the tissue. (**J**) Apparent iodine concentration in tissue versus time for a ROI in the brain stem of each mouse. Solid lines are fits of the one-dimensional diffusion equation (Equation 1) to the data points.

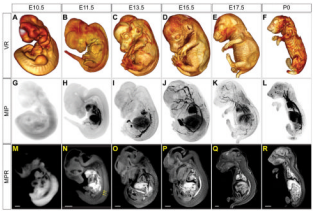


**Figure 3.**

Visualization of mouse development by micro-CT. Three viewing modes are used to generate micro-CT images of mouse embryos at stages E10.5, E11.5, E13.5, E15.5 and E17.5. Also shown is a neonate at P0 (skin removed). (**A-F**) Volume rendering (VR) windowed to show external features allows for accurate staging. (**G-L**) Maximum intensity projection (MIP) images show that blood is most intensely stained, allowing delineation of many vascular structures. (**M-R**) Representative sagittal sections generated by multi-planar reformatting (MPR) show differential staining of soft tissues in all stages except E10.5. By E11.5 even structures such as somites (arrows) can be delineated. Scale bars = 200 μm (E10.5), 800 μm (E11.5–E13.5), 1 mm (E15.5–P0).

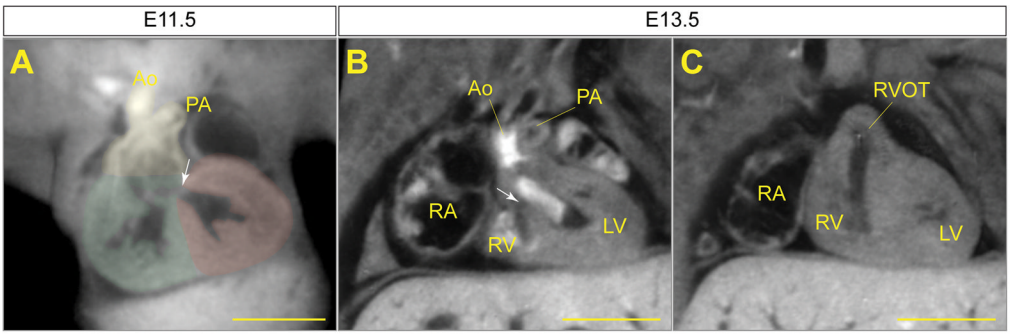


**Figure 4.**

Cardiac septation events viewed by micro-CT. MPR images at planes chosen to best illustrate septation of the conotruncus, while the ventricular septum remains incomplete. (**A**) At E11.5 the conotrucus (highlighted in yellow) is connected to both the aorta (Ao) and pulmonary artery (PA) but there is a single outlet from the presumptive right ventricle (highlighted in green). The bulboventricular foramen (arrow) is the only route of egress from the presumptive left ventricle (highlighted in red). (**B**) By E13.5, the aorta has aligned with the left ventricle (LV). The aorta and left ventricle are partially filled with blood, giving areas of high and low attenuation in the lumens. Note that the bulboventricular foramen remains patent (arrow). (**C**) In the same plane as (**B**), but more ventrally, a separate right ventricular outflow tract (RVOT) can be seen. RA- right atrium, RV- right ventricle. Scale bars = 500 μm.

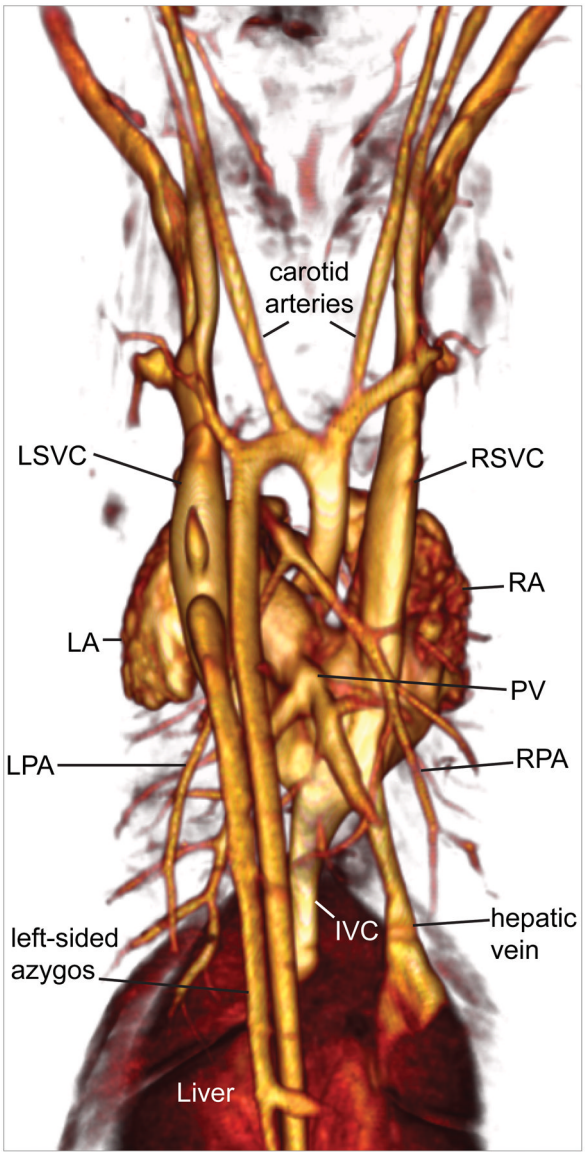


**Figure 5.**
Mouse vascular structure as viewed by micro-CT. Posterior view of VR image from a P0 mouse showing venous and arterial structures. LSVC- left superior vena cava, LA- left atrium, LPA- left pulmonary artery, IVC- inferior vena cava, RPA- right pulmonary artery, PV-pulmonary vein, RA- right atrium, RSVC- right superior vena cava.

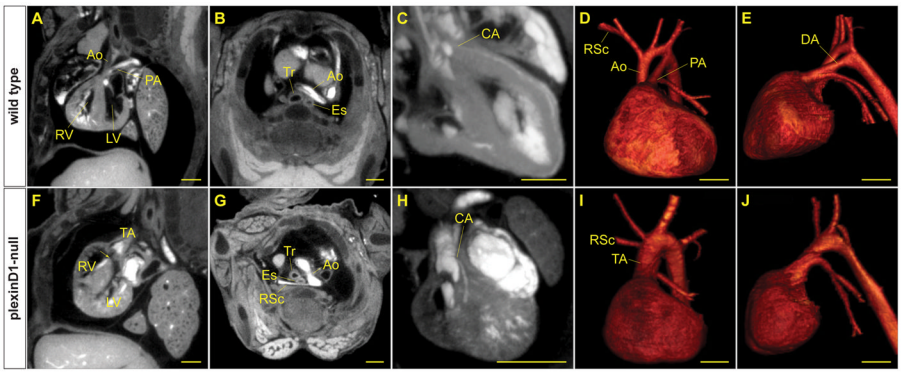


**Figure 6.**

Micro-CT demonstrates multiple cardiovascular defects in a mouse model of congenital heart disease with a known genetic lesion. MPR images of a wild type mouse (**A-C**) and a *PlexinD1* mutant mouse (**F-H**) at E17.5. Off-axis sagittal views (**A, F**) show a ventricular septal defect (arrow) below the truncal arteriosus (TA) in the mutant compared to an intact septum in the wild type. Cross-sectional views (**B, G**) show the right subclavian artery (RSc) running posterior to the trachea (Tr) and esophagus (Es) in the mutant. The wild type right subclavian artery is not in view in the same plane. (**C, H**) In the wild type, a coronary artery (CA) arises normally from the sinus of Valsalva, whereas the mutant has a coronary artery arising from the sino-tubular junction (different planes). VR images illustrate the normal anatomy (**D, E**) of the aorta (Ao) and pulmonary artery (PA), as compared to the truncus arteriosus in the mutant (**I, J**). Note the absence of the ductus arteriosus (DA) in the mutant. Atria and other tissues have been cropped away to show the base of the great vessels and branching pattern of the arteries. Scale bars = 500 μm.

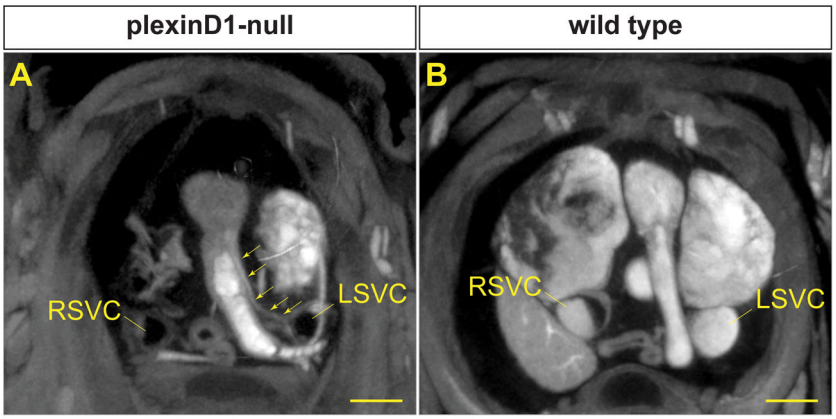


**Figure 7.**

Micro-CT reveals aberrant venous structure in a *PlexinD1* mutant. MPR image of a *PlexinD1* null (**A**) shows a structure that runs from the anterior surface of the ventricle to the left superior vena cava (LSVC) (arrows). An equivalent view of the wild type control (**B**) shows no similar structure. Note that the wild type specimen has the LSVC opacified, as it is filled with blood, whereas the mutant LSVC is shown only by the outline of the vascular wall. Similarly, the right superior vena cava (RSVC) is partially filled with blood in the wild type, but unfilled in the *PlexinD1* null. Scale bars = 500 μm.